AERODYNAMIC COMPARISON AND VALIDATION OF RANS, K-ω, STANDARD K-ε AND URANS SIMULATIONS OF FLAT PLATE FILM-COOLING

OSAMA.H.ABDULGUAD

This project report presented in partial
fulfillment of the requirements for the award of
the Degree of Master of Mechanical and Manufacturing Engineering

Faculty of Mechanical and Manufacturing Engineering
University Tun Hussein Onn Malaysia

JUNE, 2014

ABSTRACT

Film cooling has been extensively used to provide thermal protection for the external surfaces of gas turbine components. For the past 40 years, numerous number of film cooling hole designs and arrangements have been introduced. Due to broad designs and arrangements of film cooling, numerical investigation has been utilized to provide initial insight on the aerodynamics and thermal performance of the new film cooling designs or arrangements. The present work focuses on the numerical investigation of RANS and URANS analyses on a flat plate film cooling. The investigation aims to provide comparison between various turbulent models available for the Reynolds Average Navier Stokes (RANS) analyses and extended to unsteady Reynolds Average Navier Stokes (URANS). The numerical investigations make used of ANSYS CFX ver. 14 and were carried out at Reynolds Number, Re = 7,000 based on the hole diameter at blowing ratio, BR = 0.5. The results of the RANS analyses show significant influence of the turbulent models on the predicted aerodynamics and thermal performance of the film cooling. Qualitative comparison between the simulation and experimental results shows that standard k-ε produces more accurate results from the other considered turbulent models. In addition to that, results of URANS indicate limitation of RANS analyses to provide details on the eddied and vortices formation in film cooling flow structure.

CONTENTS

LIST OF TABLES

LIST OF FIGURES

NOMENCLATURE

K	Turbulent Kinetic Energy [m^2s^{-2}]
M	Blowing Ratio $\frac{\rho_c U_c}{\rho_\infty U_\infty}$
R_{ed}	Reynold's Number inside the Cooling Holes
R_{ex}	Reynold's Number of Flat Plate at Distance x from the Upstream Edge
u	Velocity Fluctuation in x-direction [ms^{-1}]
U	Velocity in x-direction [ms^{-1}]
v	Velocity fluctuation in y-direction [ms^{-1}]
V	Velocity in y-direction [ms^{-1}]
w	Velocity fluctuation in z-direction [ms^{-1}]
δ	Boundary Layer thickness [m]
η	Cooling Efficiency

LIST OF EQUATIONS

CHAPTER 1

INTRODUCTION

This chapter will provide description on gas turbine and film cooling technologies. The brief description aims to provide sufficient background of the topics for further discussion of the present work. Attention will also be paid to existing researches on film cooling technologies to develop the state of art awareness on the technologies itself.

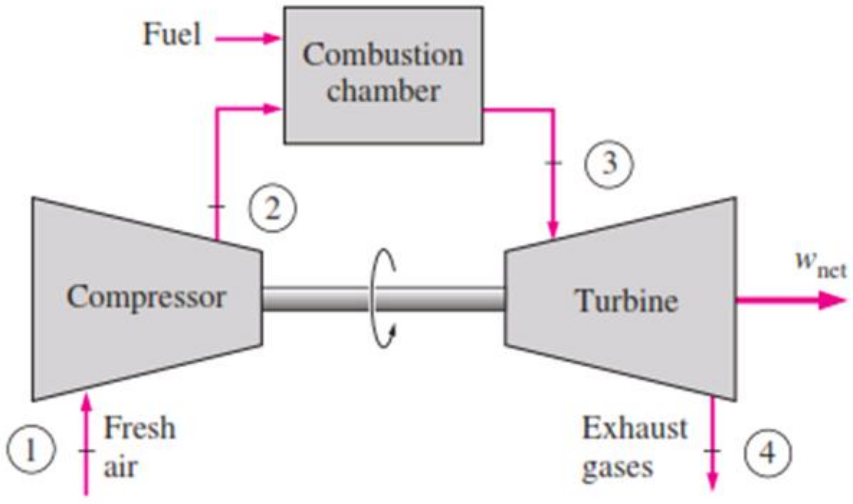

Figure 1.1: Open-cycle gas turbine engine

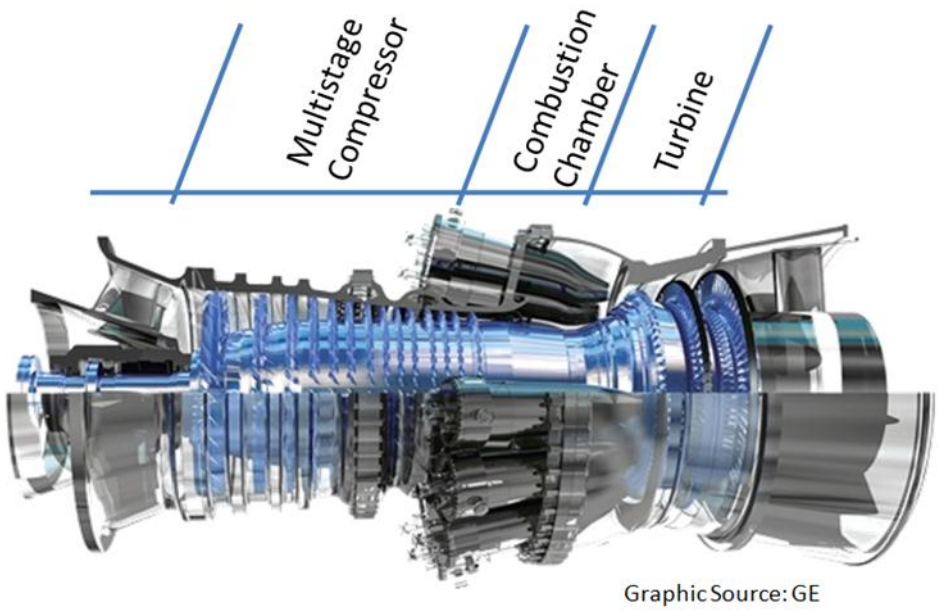

Figure 1.2: Industrial gas turbine

1.1 Background

The interest on gas turbine appeared approximately a century and half ago. But, the real success on the technology was only achieved in the year 1930 when Frank Whittle got a patent award on the jet engine. The static test of the pattern has been successfully carried out in 1937. Two years later in the year 1939, a jet engine powered flight was demonstrated by Hans von Ohain in Germany. Since then, gas turbines have been widely used in the transportation and power utility industries. Industrial gas turbine and jet engine operate in an open cycle as shown in Figure 1.1. The fresh air from the ambient will be compressed before being mixed with the fuel and burned in the combustion chamber. The high pressure and temperature flue gas will then be supplied into the turbine for power extraction process. The turbine is functioning as energy converter, converting high flow energy of the flue gas to mechanical energy. The mechanical energy (shaft rotation), will later be converted to desired form of energy. The flue gas will later release back to the ambient to complete the process. Figure 1.2 shows the real picture of an industrial gas turbine.

The working cycle of gas turbine system has been based on the ideal Brayton cycle (Figure 1.3 and Figure 1.4). The close loop of ideal Brayton cycle consists of four processes main process; a) isentropic compression (compressor), b) constant pressure heat addition (combustion chamber), c) isentropic expansion (turbine), d) constant pressure heat rejection (heat exchanger). The overall thermal efficiency of the Brayton's cycle can be presented by equation:

$$\eta_{th,Brayton} = \frac{W_{nett}}{Q_{in}} = 1 - \frac{T_4}{T_3} \qquad (1.1)$$

where W_{net}, Q_{in} ,T_3, and T_4 are the net work produce by the cycle [W], the heat supplied to the cycle [W], inlet temperature of the turbine [K], and the exit temperature of the turbine [K], respectively.

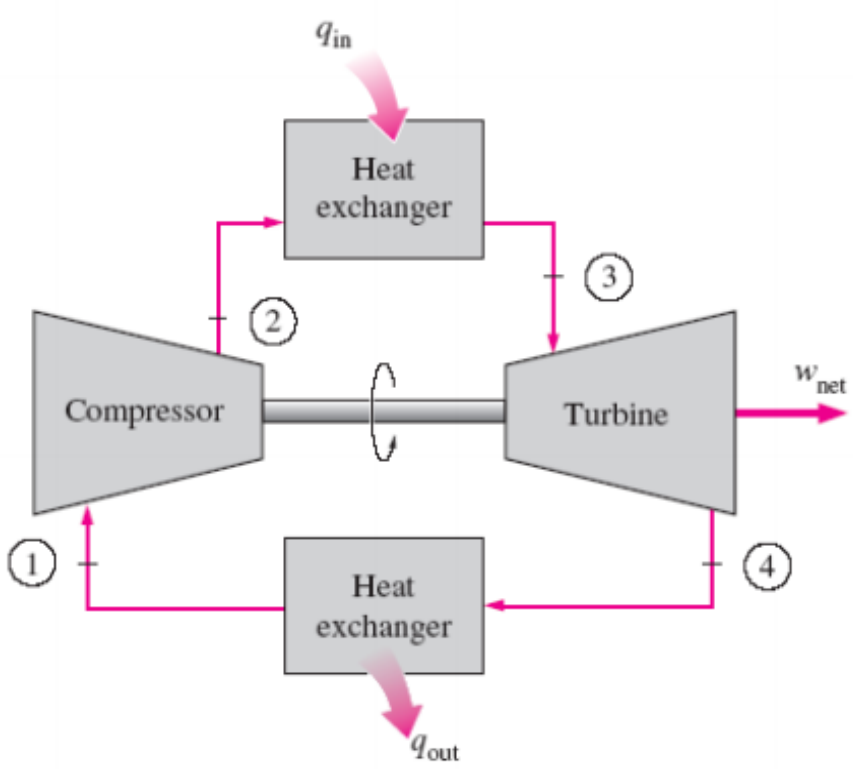

Figure1.3: Closed cycle gas turbine engine

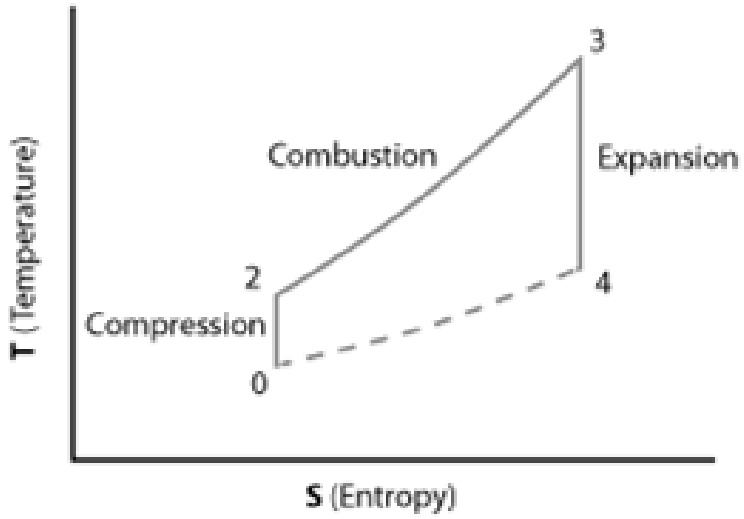

Figure 1.4: Temperature–Entropy plot of ideal Brayton cycle

Eq. (1.1) indicates higher turbine inlet temperatures produces higher overall thermal efficiency of the cycle. The increasing demand for better performance gas turbine provokes the increase of turbine inlet temperature. The modern gas turbine nowadays works at the temperature range around 1800K- 2000K, which is higher than the melting temperature of the turbine components materials. Such increasing of the turbine inlet temperature became possible because of application of cooling scheme on the turbine components. One of the cooling methods involved is film cooling technique. The working concept of film cooling lays on the injection of cold air to provide a layer of cool fluid between the hot gases and the blade surface, reducing temperature of the surface.

1.2 Problem Statement

Enormous numbers of researches have been done to improve film cooling performance. The researches focus on eliminating the counter rotating vortices effects through new hole design, holes arrangements, and introduction of passive and active devices. Due to the broad design space of film cooling, computational fluid dynamics

has been used to provide preliminary ideas on the newly proposed concept of film cooling. Therefore, it is important to acknowledge the discrepancy that could be influence by the application of different turbulent models in the steady Reynolds Average Navier Stokes (RANS) simulation. In addition to that, it is also important to acknowledge the incapability of RANS in providing accurate prediction of the formation of vortices in comparison with the unsteady Reynolds Average Navier Stokes simulation.

For the present study, six turbulence models are used to simulate a film cooling case. The model accuracy will be compared with experimental results data that are already available. In addition, further discussion will also made available on the inside hole flow phenomena predicted by all turbulent models.

1.3 Objectives Of Study

The present study aims to evaluate the capability of different turbulence models to provide the accurate prediction of aerodynamics and thermal performance of the film cooling phenomena. The objectives of the project are:

a) To compare the predicted results of different turbulent model of RANS analysis with the available experimental results;
b) To proposed the best available turbulent models of RANS analysis for film cooling study;
c) To compare the predicted results of URANS with RANS and available experimental results.

1.4 Scope Of Study

The scopes of the present study are:

i) the suimulation will be carried out using commercial computaitonal fluid dynamics package of ANSYS CFX software.
ii) the steady RANS analyses will involved six different turbulents models; SST, SSG, RNG k-ε, k-ω, and standard k-ε .
iii) the simulation will be run at Reynolds number base on hole diamater, Re = 7,000 and blowing ratio, BR = 0.5

CHAPTER 2

LITERATURE REVIEW

2.1 Introduction

In this chapter will discuss the computational models that will be used for simulation of the flow field. This is theoretical part of the work, dealt with the crucial characteristics of a different models using nowadays. The equations will be review of every model and outline their main advantages and disadvantages.

2.2 The Jet In Cross Flow

A numerous studies have been undertaken both experimentally and computationally to investigate the cooling efficiency, evolution of cooling film or influences of different geometries on the performance. Important work from experimental side has been done by Andreopoulos and Rodi [1] and Fric and Roshko [2], who characterized the evolution and main features of jet in cross flow configurations. Figure (2.1) shows a sketch of a jet in cross flow as established by Fric and Roshko [2]

Containing four principal types:

- Shear layer vortices
- Counter-rotating vortex pair
- Horseshoe vortex
- Wake vortices

The conclusions were drawn from experiments with velocity ratios between 2 and 10 as well as cross flow Reynolds numbers in the range from 3 800 up to 11 400[3].

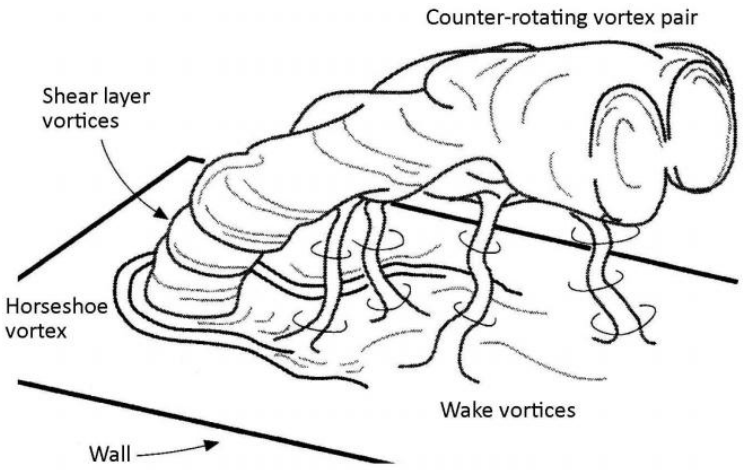

Figure 2.1: Main vortical structures as proposed by Fric & Roshko [2]

A lot of experimental work has been done by the group of Crawford in the field of the application of jets in cross flow for film cooling applications [4-8]. They measured film cooling effectiveness for full-coverage film cooling configurations [4-6], as well as aerodynamic measurements [7] and film cooling effectiveness [8] for single row configurations. Goldstein [9] gives an introduction to film cooling, which includes several cooling methods and explains important parameters in film cooling flows. He also

gives an overview of work done in the field during the 1950s and 60s. A bibliography done in CFD of film cooling flows is given by Kercher [10]. It includes references from 1971 to 1996. Bacchi and Facchini [11] used a modified k-ε model to simulate flat-plate film cooling in order to overcome the typical errors of standard two-equation models in film cooling. These errors are an underpredicted lateral jet spreading and an overpredicted jet penetration into the mainstream. These systematical errors arise from the assumption of isotropic turbulence. Yavuzkurt [12-13] use the standard, RNG and realizable k-ε model and the k-ω model for film cooling from inclined holes. Their results show that all used models give acceptable results for a low blowing ratio of M=0.5 but completely fail to predict the cooling effectiveness for a large blowing ratio of M=1.5, especially in the area just downstream of the cooling hole (x/D<8). Furthermore their studies show that the results strongly depend on the used mesh. For a hexahedral mesh the results are clearly better than for a mesh which is partly meshed tetrahedral and partly hexahedral. Harrison and Bogard [14] used three turbulence models, namely the standard k-ε, the standard k-ω and a Reynolds Stress model (RSM) to simulate film cooling from a 30 degree inclined hole. Their results show that the standard k-ω model gives best results for the laterally averaged cooling effectiveness, but at the same time gives the worst agreement with the experiments for the centerline effectiveness.

2.3 Turbulence Models

2.3.1 The SST Model

The SST k-ω turbulence model [Menter 1993] is a two- equation eddy-viscosity model which has become very popular. The shear stress transport (SST) formulation combines the best of two worlds. The use of a k-ω formulation in the inner parts of the boundary layer makes the model directly usable all the way down to the wall through the viscous sub-layer; hence the SST k-ω model can be used as a Low-Re turbulence model without any extra damping functions. The SST formulation also switches to a k-ε behavior in the free-stream and thereby avoids the common k-ω problem that the model is too sensitive to the inlet free-stream turbulence properties. Authors who use the SST k-ω

model often merit it for its good behavior in adverse pressure gradients and separating flow. The SST k-ω model does produce a bit too large turbulence levels in regions with large normal strain, like stagnation regions and regions with strong acceleration. This tendency is much less pronounced than with a normal k-ε model though [15].

Kinematic Eddy Viscosity

$$v_T = \frac{a1\,k}{max(a1\omega, SF2)} \tag{2.1}$$

Turbulence Kinetic Energy

$$\frac{\partial k}{\partial t} + U_j \frac{\partial k}{\partial x_j} = P_k - \beta^* k\omega + \frac{\partial}{\partial x_i}\left[(v + \sigma_k v_T)\frac{\partial k}{\partial x_j}\right] \tag{2.2}$$

Specific Dissipation Rate

$$\frac{\partial \omega}{\partial t} + U_j \frac{\partial \omega}{\partial x_j} = \alpha S^2 - \beta\omega^2 + \frac{\partial}{\partial x_j}\left[(v + \sigma_\omega v_T)\frac{\partial \omega}{\partial x_j}\right] + 2(1 - F_1)\sigma_{\omega 2}\frac{1}{\omega}\frac{\partial k}{\partial x_i}\frac{\partial \omega}{\partial x_i} \tag{2.3}$$

Closure Coefficients and Auxiliary Relations

$$F_2 = tanh\left[\left[max\left(\frac{2\sqrt{k}}{\beta^*\omega y}, \frac{500\,v}{y^2\omega}\right)\right]^2\right] \tag{2.4}$$

$$P_k = min\left(\tau_{ij}\frac{\partial U_i}{\partial x_j}, 10\beta^* k\omega\right) \tag{2.5}$$

$$F_1 = \tanh\left\{\left\{min\left[max\left(\frac{\sqrt{k}}{\beta^*\omega y}, \frac{500\,v}{y^2\omega}\right), \frac{4\sigma_{\omega 2}k}{CD_{K\omega}y^2}\right]\right\}^4\right\} \tag{2.6}$$

$$CD_{k\omega} = \max\left(2\rho\sigma_{\omega 2}\frac{1}{\omega}\frac{\partial k}{\partial x_i}\frac{\partial \omega}{\partial x_i}, 10^{-10}\right) \tag{2.7}$$

Each of the constants is a blend of an inner (1) and outer (2) constant, blended via:

$$\phi = \phi_1 F_1 + \phi_2 (1 - F_1) \tag{2.8}$$

Table 2.1: Typical values for the constants in the equations

α_1	α_2	β_1	β_2	β^*	σ_{k1}	σ_{k2}	$\sigma_{\omega 1}$	$\sigma_{\omega 2}$
5/9	0.44	-3/40	0.0828	9/100	0.85	1	0.5	0.856

2.3.2 The Reynolds Stress Model by Speziale, Sarkar and Gatski (SSG)

The transport equation of the Reynolds stresses can be derived by multiplying the momentum equation with the fluctuating velocity components and time averaging the product (Wilcox, 1993):

$$\frac{\partial \overline{u_i' u_j'}}{\partial_t} + \overline{U_k} \frac{\partial \overline{u_i' u_j'}}{\partial x_k} = P_{ij} + \frac{\partial}{\partial x_k}\left(D_{ijk}^{\nu}\right) + \frac{\partial}{\partial x_k}\left(D_{ijk}^{t}\right) + \Pi_{ij} - \varepsilon_{ij} \tag{2.9}$$

The production term is defined using the exact form

$$P_{ij} = -\left[\overline{u_j' u_k'} \frac{\partial \overline{U_i}}{\partial x_k} + \overline{u_i' u_k'} \frac{\partial \overline{U_J}}{\partial x_k}\right] \tag{2.10}$$

Molecular diffusion also follows the exact definition

$$D_{ijk}^{\nu} = \nu \frac{\partial}{\partial x_k}\left(\overline{u_i' u_J'}\right) \tag{2.11}$$

The model for the turbulent diffusion

$$D_{ijk}^{t} = C_s \frac{k}{\varepsilon}\left[\overline{u_k' u_J'} \frac{\partial \overline{u_i' u_J'}}{\partial x_i}\right] \tag{2.12}$$

Many models for the pressure - strain term have been developed since the pioneering work of Launder, Reece, and Rodi. A general form is given by

$$\Pi_{ij} = -C_1 b_{ij} + C_1'\varepsilon\left[b_{ik}b_{kj} - \frac{1}{3}b_{mn}b_{mn}\delta_{ij}\right] + C_2 k S_{ij} + C_3 k\left[b_{ik}S_{ik} + b_{jk}S_{ik} - \frac{2}{3}b_{mn}S_{mn}\delta_{ij}\right] + C_4 k\left[b_{ik}W_{jk} + b_{jk}W_{ik}\right] \quad (2.13)$$

Where the stress anisotropy tensor is given by

$$b_{ij} = \frac{\overline{u_i'u_j'}}{2k} - \frac{1}{3}\delta_{ij} \quad (2.14)$$

The strain rate tensor is defined as

$$S_{ij} = \frac{1}{2}\left[\frac{\partial u_i}{\partial x_j} + \frac{\partial u_j}{\partial x_i}\right] \quad (2.15)$$

The rotation tensor is given by

$$W_{ij} = \frac{1}{2}\left[\frac{\partial u_i}{\partial x_j} + \frac{\partial u_j}{\partial x_i}\right] \quad (2.16)$$

If the turbulence is assumed to be locally isotropic then the dissipation term in the incompressible form of the second moment equation can be reduced to

$$\varepsilon_{ij} = \frac{2}{3}\,\varepsilon\,\delta_{ij} \quad (2.17)$$

Where **ε** is the total rate of energy dissipation.

A transport equation for the dissipation must also be solved to close the system of equations. The dissipation equation can be written as

$$\frac{\partial \varepsilon}{\partial t} + \overline{U_k}\frac{\partial \varepsilon}{\partial x_k} = C_{\varepsilon 1}\frac{\varepsilon}{k}P_\varepsilon - C_{\varepsilon 2}\frac{\varepsilon^2}{k} + \frac{\partial}{\partial x_k}\left[\nu\frac{\partial \varepsilon}{\partial x_k}\right] + \frac{\partial}{\partial x_i}\left(D_{\varepsilon j}^t\right) \quad (2.18)$$

The first term on the right hand side of equation is the production of dissipation. The second term represents the dissipation of the dissipation. The last two terms are the

molecular and turbulent diffusion of dissipation respectively [16]. The production of dissipation is given by

$$P_\varepsilon = -\left[\overline{u_l' u_j'} \frac{\partial \overline{U_l}}{\partial x_j}\right] \tag{2.19}$$

The dissipation equation turbulent diffusion term is modeled by

$$D_{\varepsilon j}^t = C_\varepsilon \left[\frac{k}{\varepsilon} \overline{u_k' u_l'} \frac{\partial \varepsilon}{\partial x_j}\right] \tag{2.20}$$

Table 2.2: Typical values for the constants in the equations for the Speziale-Sarker-Gatski (SSG) RSM models [16]

Model	C_1	C_1'	C_2	C_3	C_4	C_s	$C_{\varepsilon 1}$	$C_{\varepsilon 2}$	C_ε
SSG	3.4+1.8P/ε	4.2	0.8-1.3$\left(b_{ij} b_{ij}\right)^{1/2}$	1.25	0.4	0.11	1.44	1.83	0.11

2.3.3 RNG K-Ɛ Model

The RNG model was developed using Re-Normalisation Group (RNG) methods by Yakhot and Orsag to renormalise the Navier-Stokes equations, to account for the effects of smaller scales of motion. In the standard k-epsilon model the eddy viscosity is determined from a single turbulence length scale, so the calculated turbulent diffusion is that which occurs only at the specified scale, whereas in reality all scales of motion will contribute to the turbulent diffusion. The RNG approach, which is a mathematical technique that can be used to derive a turbulence model similar to the k-epsilon, results in a modified form of the epsilon equation which attempts to account for the different scales of motion through changes to the production term.

$$\frac{\partial(\rho k)}{\partial t} + div(\rho kU) = div\left[\alpha_\kappa \mu_{eff}\ grad\ k\right] + 2\mu_t E_{ij}.E_{ij} - \rho\varepsilon \quad (2.21)$$

$$\frac{\partial(\rho\varepsilon)}{\partial t} + div\ (\rho\varepsilon U) = div\left[\alpha_\varepsilon \mu_{eff}\ grad\ \varepsilon\right] + C_{1\varepsilon}^{*}\frac{\varepsilon}{k}\ 2\ \mu_t E_{ij}.E_{ij} - C_{2\varepsilon}\rho\frac{\varepsilon^2}{k} \quad (2.22)$$

Where:

$$\mu_{eff} = \mu + \mu_t \quad , \quad \mu_t = \rho C_\mu \frac{k^2}{\varepsilon} \quad , \quad C_{1\varepsilon}^{*} = C_{1\varepsilon} - \frac{\eta(1-\eta/\eta_o)}{1+\mathrm{B}\eta^3} \quad , \quad \eta = (2E_{ij}.\ E_{ij})^{1/2}\frac{\kappa}{\varepsilon}$$

$$\eta_o = 4.377 \quad , \quad B = 0.012$$

Table 2.3: The fine constants contained in the equation [17]

Model	C_μ	α_κ	α_ε	$C_{1\varepsilon}$	$C_{2\varepsilon}$
Rodi	0.0845	1.39	1.39	1.42	1.68

Only the constant B is adjustable, the above value is calculated from near wall turbulence data. All other constant are explicitly computed as part of the RNG process. The model is one of the main sources of accuracy limitations for standard version of the K-ε model and the RSM in flows that experience large rates of deformation. Also the model is very good predictions of the flow over a backward-facing step. But it is slightly more expensive of the standard version. [18]

2.3.4 K-ω Model (Wilcox's)

The basic equations for this two-equation model are:

$$\frac{\partial(\rho \mathrm{k})}{\partial \mathrm{t}} + \frac{\partial(\rho \mathrm{u_j k})}{\partial \mathrm{x_j}} = \mathrm{P} - \beta^{*}\rho\omega k + \frac{\partial}{\partial x_i}\left[\left(\mu + \sigma_k\frac{\rho k}{\omega}\right)\frac{\partial k}{\partial x_j}\right] \quad (2.23)$$

$$\frac{\partial(\rho\omega)}{\partial t}+\frac{\partial(\rho u_j\omega)}{\partial x_j}=\frac{\gamma\omega}{k}\,P-\beta\rho\omega^2+\frac{\partial}{\partial x_j}\left[\left(\mu+\sigma_\omega\frac{\rho k}{\omega}\right)\frac{\partial\omega}{\partial x_j}\right] \quad (2.24)$$

And the turbulent eddy viscosity is computed from:

$$\mu_t=\frac{\rho k}{\omega} \quad (2.25)$$

Table 2.4: The difference in the values taken by some of the variables

σ_k	σ_ω	β^*	β	γ
0.5	0.5	0.99	3/4	5/9

- The model uses two equations. In this model **ω** is an inverse time scale what associated with the turbulence
- This model solves two additional PDES:

1. A modified version of the **k** equation used in the k-ε model
2. A transport equation for **ω**

- Its numerical behavior is similar to that of the k-ε models [18]

Near wall treatment for low-Reynolds number amputations is one of the advantages of the k-ω formulation. Here "low-Reynolds" refers to the turbulent Reynolds number, which is low in the viscous sub-layer, not the device Reynolds number. In other words "low-Reynolds number computations" means the near wall mesh is fine enough to resolve the laminar (viscous) part of boundary layer which is very close to the wall [18]

2.3.5 Standard K-Ɛ Model

It has two model equations one for K and other one for Ɛ. k and Ɛ are used to define the Velocity scale ϑ and length scale l representative of the large scale turbulence.

$$\vartheta = k^{1/2} \qquad l = \frac{k^{3/2}}{\varepsilon}$$

The standard model uses the following transport equations:

K equation:

$$\frac{\partial(\rho k)}{\partial t} + div(\rho k U) = div\left[\frac{\mu_t}{\sigma_k}\, grad\, k\right] + 2\mu_t E_{ij}.E_{ij} - \rho\varepsilon \tag{2.26}$$

Ɛ equation:

$$\frac{\partial(\rho\varepsilon)}{\partial t} + div\,(\rho\varepsilon U) = div\left[\frac{\mu_t}{\sigma_\varepsilon}\, grad\, \varepsilon\right] + C_{1\varepsilon}\frac{\varepsilon}{k}\, 2\,\mu_t E_{ij}.E_{ij} - C_{2\varepsilon}\rho\frac{\varepsilon^2}{k} \tag{2.27}$$

The turbulent eddy viscosity is:

$$\mu_t = C\rho\,\vartheta\, l = \rho\, C_\mu\, \frac{k^2}{\varepsilon} \tag{2.28}$$

Table 2.5: The fine constants contained in the equation [18]

C_μ	σ_k	σ_ε	$C_{1\varepsilon}$	$C_{2\varepsilon}$
0.009	1.00	1.30	1.44	1.92

k-ε Model is the simplest turbulence model for which only initial or boundary condition need to be supplied. This model also is an excellent performance for many industrially relevant flows. It is well established and the most widely validated turbulence model. From another side, it is more expensive to implement than mixing length model. It also has the poor performance in a variety of important cases such as some unconfined flows; flows with large extra strains (e.g. curved boundary, swirling flows); rotating flow and fully developed flows in non-circular ducts. [18]

2.3.6 The Unsteady RANS (URANS) Model

The governing equations for URANS:

Continuity:

$$\frac{\partial \mathrm{U}_i}{\partial x_i} = 0 \tag{2.29}$$

Momentum:

$$\frac{\partial U_i}{\partial t} + U_j \frac{\partial U_i}{\partial x_j} = -\frac{1}{\rho} \frac{\partial P}{\partial x_j} + \nu \frac{\partial^2 \mathrm{U}_i}{\partial x_j \partial x_j} - \frac{\partial}{\partial x_j} u_i u_j \tag{2.30}$$

Where the Reynolds stress term is approximated using the Boussinesque approximation as:

$$u_i u_j = \frac{2}{3} K \delta_{ij} - v_t \left[\frac{\partial \mathrm{U}_i}{\partial x_j} + \frac{\partial \mathrm{U}_j}{\partial x_i}\right] \tag{2.31}$$

The eddy viscosity is written as:

$$v_t = C_\mu f_\mu \frac{k^2}{\varepsilon} \tag{2.32}$$

The modeled transport equations for k and Ɛ are given as:

K equations:

$$U_j \frac{\partial k}{\partial x_j} = \frac{\partial}{\partial x_j}\left[\left[v + \frac{v_t}{\sigma k}\right]\frac{\partial k}{\partial x_j}\right] + \left[-u_i u_j \frac{\partial U_i}{\partial x_j}\right] - \varepsilon \tag{2.33}$$

Ɛ equations:

$$U_J \frac{\partial \varepsilon}{\partial x_j} = \frac{\partial}{\partial x_j}\left[\left[v + \frac{v_t}{\sigma_\varepsilon}\right]\frac{\partial \varepsilon}{\partial x_j}\right] + C_{\varepsilon 1} \frac{\varepsilon}{k}\left[-u_i u_j \frac{\partial U_I}{\partial x_j}\right] - C_{\varepsilon 2} f_2 \frac{\varepsilon^2}{k} \tag{2.34}$$

It is therefore expected that for an inherently unsteady problem like the film cooling of turbine blades, URANS can be a viable and inexpensive alternative to DNS and LES [20].

CHAPTER 3

METHODOLOGY

3.1 Introduction

This chapter will provide the information on the methodology for the research it will covers on ANSYS CFX software, Flow chart, CFD simulation, unsteady case, and Film cooling effectiveness.

3.2 ANSYS CFX

ANSYS CFX is commercial finite-element analysis software with the capability to analyze a wide range of different problems. The program was created to achieve more accurate results in a short time and reduce financial costs on the stage of components or materials producing. It contains five important parts:

a) Design modeler
b) Meshing
c) Pre-CFX
d) CFX processing
e) Post CFX

3.3 Methodology Flowchart

A flow chart represents the process of the methodology for research and the steps to be carried out even to obtain the results and discussion.

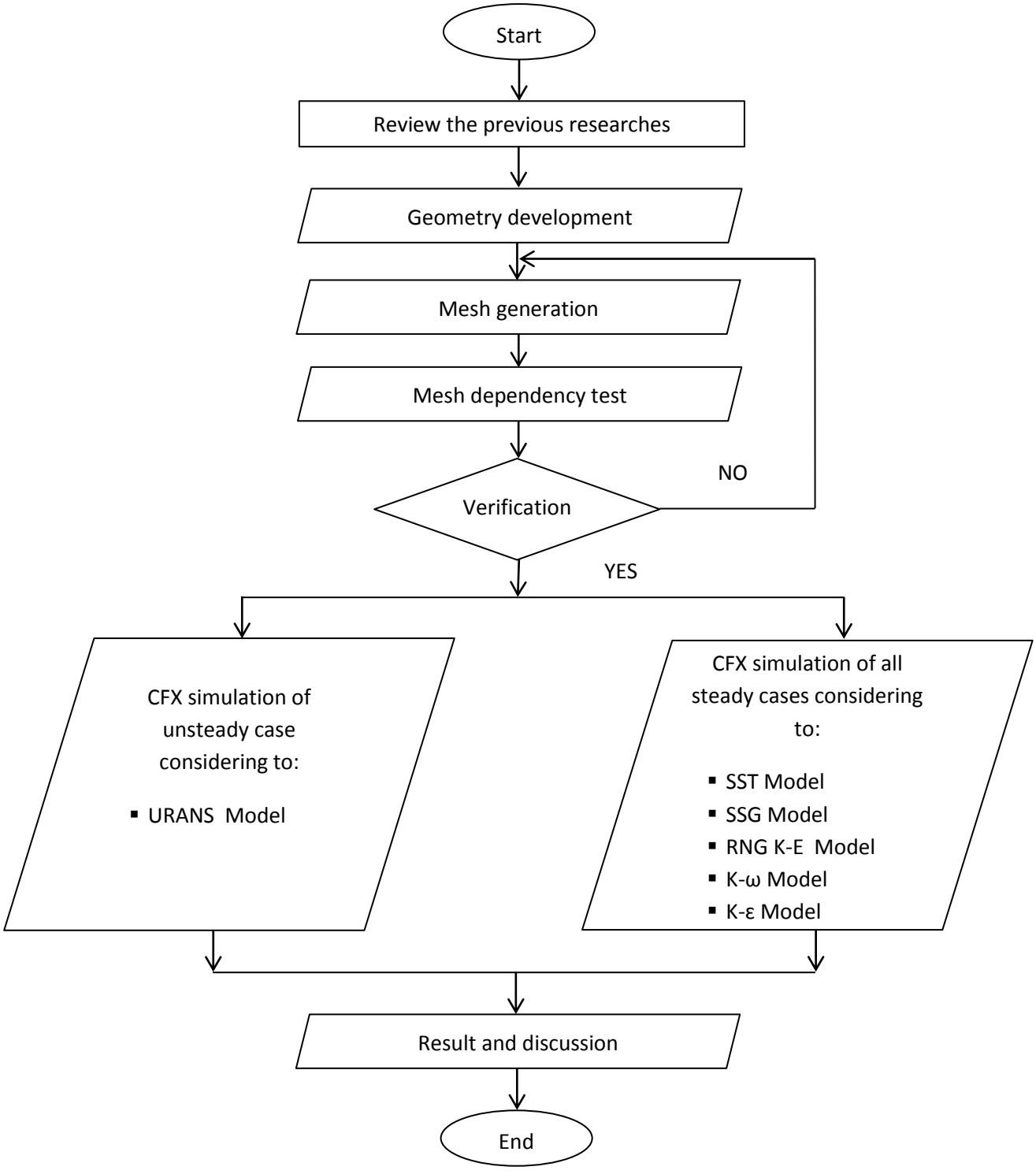

Figure 3.1: Methodology Flowchart

3.4 Computational Fluid Dynamics (CFD) Simulation

CFD uses the numerical methods and algorithms from fluid mechanics to analyze fluid flow problems. It will take some time to calculate the relevant data to simulate the interaction between liquids and gases by defining the boundary conditions. This section will be discussing on Geometry, Meshing, and Boundary conditions.

3.4.1 Geometry

The geometrics will correspond to the experiments of Pietrzyk [7]. In the experiment the main flow goes over the flat plate with a row of 11 cylindrical cooling holes, which are 35 degree inclined against the plate. The lateral spacing between the holes is 3 hole diameters and hole length to diameter ratio is L/D=3.5.The cooling holes are fed with air from a plenum. The cooling holes have a diameter of 12.7 mm.The computational domain is laterally restricted to include just one cooling hole in the unsteady simulations and half a cooling hole in the steady simulations. The upstream boundary arranges 10 diameters from the leading edge of the cooling hole and the downstream boundary arranges 20 diameters behind the leading edge of the hole. The height above the flat plate is 5 diameters. The research includes two geometrics:

- With the half cooling hole in the steady simulation (Figure 3.2)

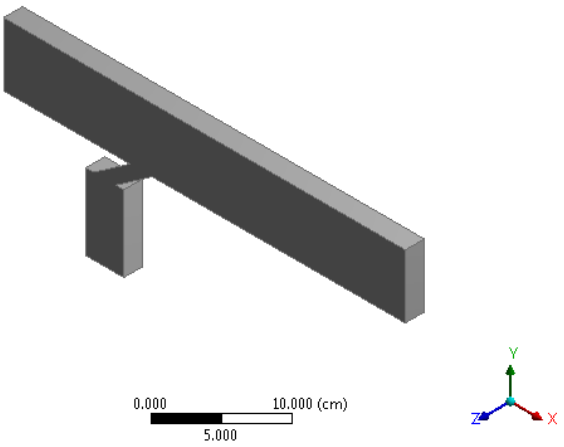

Figure3.2: The steady simulation

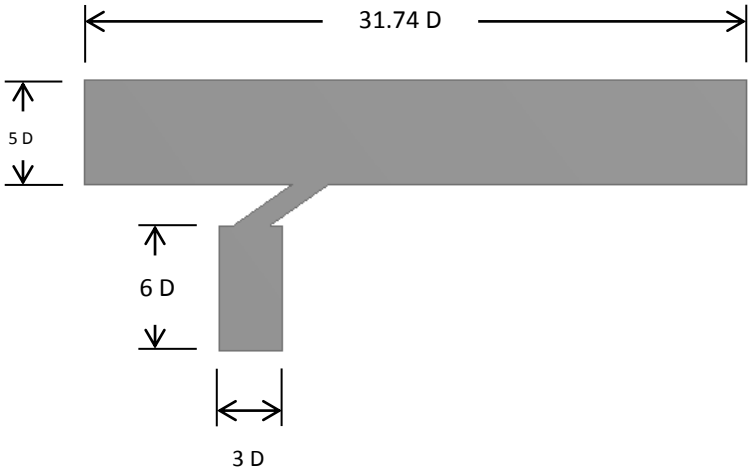

Figure3.2a: The steady simulation Side view

Figure3.2b: The steady simulation Top view

- With a one cooling hole in the unsteady simulations (Figure 3.3)

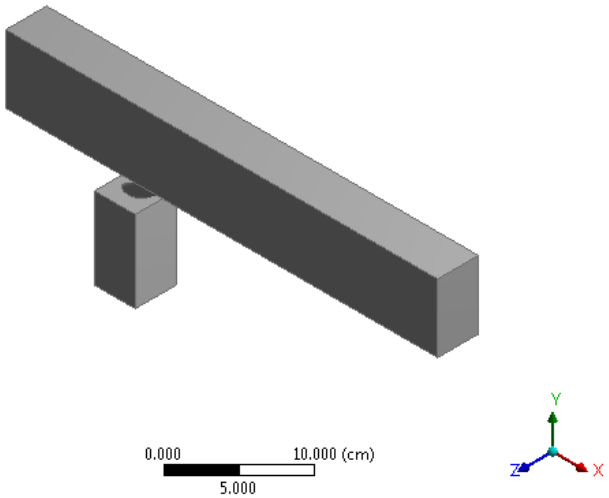

Figure 3.3: The unsteady simulation

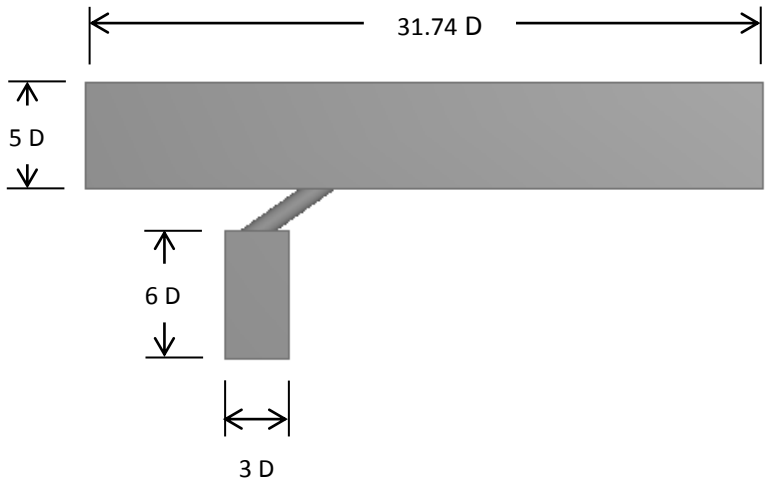

Figure3.3a: The unsteady simulation Side view

Figure3.3b: The unsteady simulation Top view

3.4.2 Meshing

The purpose of the mesh generator is to decompose the flow domain into control volumes. The shapes of control volumes depend on the capabilities of the solver. Structured-grid codes use quadrilaterals in 2-d and hexahedra in 3-d flows. Unstructured-grid solvers often use triangles 2-d or tetrahedra 3-d. The hybrid combines both of the structured and unstructured mesh.

- Structured grids are those whose control volumes can be indexed by (i,j,k) for i=1,…,n , j=1,…,n , and k=1,…,n . Each structured block of control volume, even if curvilinear, can be distorted by a coordinate transformation into a cube. Structured meshes can be used for many practical flow configurations.
- Unstructured meshes can accommodate completely arbitrary geometries .Grid generator and plotting routines for such meshes are also very complex.
- Hybrid mesh consists of the structured and unstructured mesh. This is depending of geometric design where some part of it need to structured and unstructured for another.

In this research generally the grid has been carried out hybrid type (Figure 3.4-3.7) that means contains the structured and unstructured mesh. The body has built unstructured, but the structured mesh has inflation from wall surface because it needs more critical meshing.

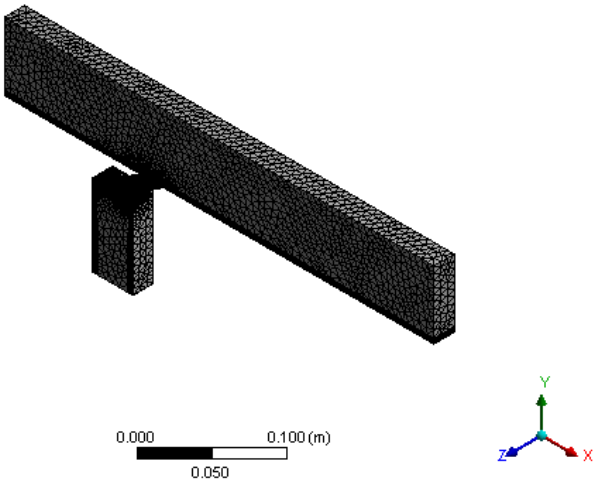

Figure 3.4: Meshing model for steady simulation

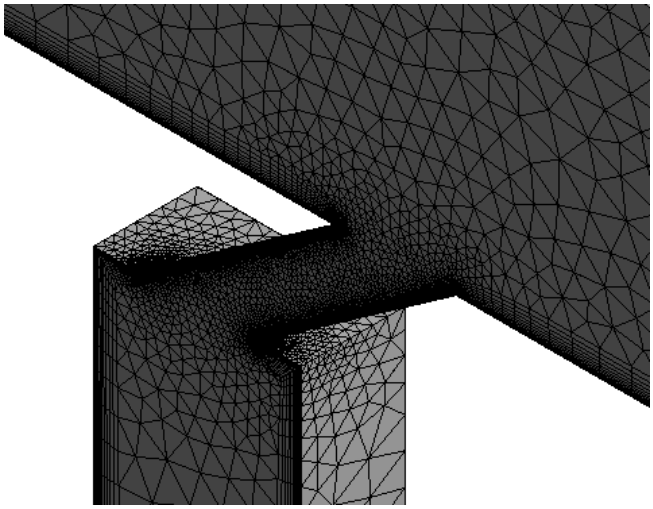

Figure 3.5: Hybrid type of meshing for steady simulation

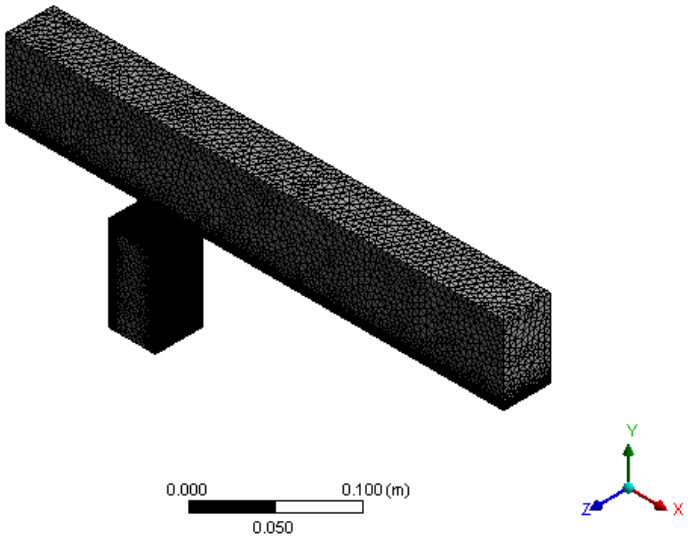

Figure 3.6: Meshing model for unsteady simulation

References

[1] Andreopoulos, J., Rodi, W. (1984). *Experimental Investigation of Jets in a Crossflow*. J. of Fluid Mechanics, 138, pp. 93-127.

[2] Fric, T.F., Roshko, A. (1994). *Vortical Structure in the Wake of Transverse Jet*. J. of Fluid Mechanics, 279, pp. 1-47.

[3] A. Sau, T. Sheu, R. Hwang, and W. Yang (2004). *Three-Dimensional Simulation of Square Jets in Cross-Flows.* Physical Review E, 69.

[4] Crawford, M.E., Kays, W.M., Moffat, R.J. (1980). *"Full-Coverage Film-Cooling on Flat, Isothermal Surfaces: A Summary Report on Data and Predictions"*. NASA Paper No. CR3219.

[5] Crawford, M.E., Kays, W.M., Moffat, R.J. (1980). *"Full-Coverage Film Cooling; Part 1 Comparison of Heat Transfer Data for Three Injection Angles"*, ASME Paper No. 80/GT/43.

[6] Crawford, M.E., Kays, W.M., Moffat, R.J. (1980). *"Full-Coverage Film Cooling; Part 2 Heat Transfer Data and Numerical Simulation"*, ASME Paper No. 80/GT/44.

[7] Pietrzyk, J.R., Crawford, M.E., Bogard, D.G. (1988). *"Hydrodynamic Measurements of Jets in Crossflow for Gas Turbine Film Cooling Applications"*, ASME Paper No. 88/GT/174.

[8] Sinha, A.K., Bogard, D.G., Crawford, M.E. (1990). *"Film Cooling Effectiveness Downstream of a Single Row of Holes with Variable Density Ratio"*, ASME Paper No. 90/GT/43.

[9] Goldstein, R.J. (1971).*"Film Cooling"*, Advances in Heat Transfer, 7, pp. 321-380.

[10] Kercher, D.M. (1998). *"A Film-Cooling CFD Bibliography"*, Int. J. of Rotating Machinery (1971-1996), 4, No. 1, pp. 61-72.

[11] Bacci, A., Facchini B. (2007). *"Turbulence Modeling for the Numerical Simulation of Film and Effusion Flows"*. ASME TurboExpo, Montreal, Canada. Paper No. GT2007-27182.

[12] Yavuzkurt, S., Hassan, J. (2007). *"Evaluation of Two-Equation Models of Turbulence in Predicting Film Cooling Performance Under High Free Stream Turbulence"*. ASME TurboExpo, Montreal, Canada.Paper No. GT2007-27184.

[13] Yavuzkurt, S., Habte, M. (2008). *"Effect of Computational Grid on Performance of Two-Equation Models of Turbulence for Film Cooling Applications"*. ASME TurboExpo, Berlin, Germany. Paper No. GT2008-50153.

[14] Harrison, K.L., Bogard, D.G. (2008). *"Comparison of RANS Turbulence Models for Prediction of Film Cooling Performance"*. ASME TurboExpo, Berlin, Germany. Paper No. GT2008-51423.

[15] Menter, F. R. (August 1994). *"Two-Equation Eddy-Viscosity Turbulence Models for Engineering Applications"*. AIAA Journal, Vol. 32, No. 8, pp. 1598-1605.

[16] Journal of Physics: Conference Series 318(2011)042031, 13th European Turbulence Conference (ETC 13).

[17] V. C. PATEL, W. RODI, and G. SCHEUERER. (1985). *"Turbulence models for near-wall and low Reynolds number flows - A review"*. AIAA Journal, Vol. 23, No. 9, pp. 1308-1319.

[18] DAVID C. WILCOX. *"Comparison of two-equation turbulence models for boundary layers with pressure gradient"*. AIAA Journal, Vol. 31, No. 8 (1993). pp. 1414-1421.

[19] Versteeg, H.K., Malalasekera, W. (1995). *"The Introduction to Computational Fluid Dynamics. The Finite Volume Method"*. Longman Scientific and Technical, New York, United States.

[20] Asif Hoda, B.S. (1997). *"Turbulence Modeling for Film Cooling Flows"*. Birla Institute of Technology, India.

[21] Pietrzyk, J.R. (1989). *"Experimental Study of the Interaction of Dense Jets with a Crossflow for Gas Turbine Applications"*, PhD Thesis, University of Texas at Austin.